ACS Energy LETTERS

Open Access

This article is licensed under CC-BY 4.0

http://pubs.acs.org/journal/aelccp

Letter

Electrochemical Charging of MAX Phases and Their Hydrogen Storage Mechanisms

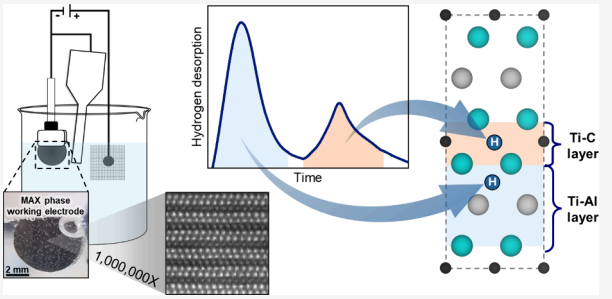
Rebeca Miyar,* Adam C. Miles, Michal Fečík, Manoj Prabhakar, Guillaume Hachet, Lilian Vogl, Dierk Raabe, Gerhard Dehm, Yug Joshi, Maxim Sokol, Jochen M. Schneider, Barak Ratzker, and Maria Jazmin Duarte*

Cite This: *ACS Energy Lett.* 2026, 11, 4457−4464

Read Online

ACCESS | Metrics & More | Article Recommendations | Supporting Information

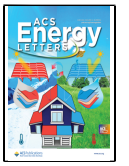
ABSTRACT: MAX phases, layered ternary transition metal carbides/nitrides, are proposed as solid-state hydrogen storage materials offering tunable intrinsic trapping sites owing to their unique atomically layered structure; however, experimental validation remains limited. Here, we present a systematic investigation of electrochemical hydrogen charging in Ti_2AlC and Ti_3AlC_2, revealing that the hydrogen storage behavior correlates to the different ratios of metal/carbide layers. Thermal desorption spectroscopy (TDS) and cyclic voltammetry (CV) measurements revealed two distinct hydrogen desorption peaks, associated with intermediate and deep trapping sites. Notably, Ti_2AlC stored ∼60% in intermediate traps and ∼40% in deep traps, while Ti_3AlC_2 showed the opposite trend. Density functional theory (DFT) calculations verify that the intermediate and deep trapping sites correspond to interstitials in the Ti−Al layer and carbon vacancies in the Ti−C layer, respectively. These findings provide insight into the layered-dependent hydrogen trapping, retention, and release in MAX phases, opening new pathways toward trap-engineered hydrogen storage in layered materials.



Hydrogen storage is a main challenge in the transition to clean energy systems due to the lack of safe, scalable, and efficient storage technologies. Conventional methods, such as high-pressure tanks and liquid hydrogen storage, present considerable safety challenges and high costs,[1,2] thus drawing increasing interest to solid-state hydrogen storage as an energy-efficient and safer alternative.[3,4] Such solid-state storage materials can store hydrogen through different hydride phases[5,6] or sorption mechanisms in various trapping sites.[7,8] Hydride-based storage offers high capacity and relatively stable long-term applications, especially stationary storage, where hydrogen release can occur at higher temperatures[9−11] (>300 °C). However, hydride materials are severely limited by their slow kinetics, unattractive hydrogen release temperatures that are mostly too high, viz., above the desirable range for mobile applications[12,13] (∼150−200 °C), and especially by their susceptibility to rapid degradation upon charge/release cycles.[6,14,15] On the other hand, sorption-based storage can enable more versatile charging/release of hydrogen with high stability and cyclability. However, these also face challenges, such as limited volumetric capacity and the difficulty of achieving efficient and reversible hydrogen release, which are tightly related to the trapping mechanisms in each material system.[7,16−21] Hence, research and development of such materials require a deep understanding of their trapping sites, permeation behavior, and desorption conditions.

MAX phases, a family of layered ternary transition metal carbides and nitrides, have recently attracted attention as potential hydrogen storage materials due to their unique nanolaminated, atomically layered structure.[22,23] These materials follow the general chemical formula $M_{n+1}AX_n$, where M is an early transition metal, A corresponds to a group 13 or 14 element, and X represents carbon and/or nitrogen, with n typically being 1, 2, or 3, defining different MAX phases, such as Ti_2AlC and Ti_3AlC_2.[22,24−28] The atomically layered structure of MAX phases offers an abundance of intrinsic trapping sites associated with the inherent crystal structure, mechanistically differing them from many conventional hydrogen storage materials that evolve and degrade over repeated storage−release cycles.[3,4] Theoretical studies have discussed the hydrogen storage potential of MAX phases, mainly showing that hydrogen prefers to occupy interstitial sites along the M−A interfaces, where the local coordination environment and electronic structure provide abundant energetically favorable binding sites.[29,30] While these

Received: February 25, 2026
Revised: April 23, 2026
Accepted: May 1, 2026
Published: May 6, 2026



Downloaded via 84.118.51.191 on June 17, 2026 at 10:20:52 (UTC).
See https://pubs.acs.org/sharingguidelines for options on how to legitimately share published articles.

© 2026 The Authors. Published by American Chemical Society

https://doi.org/10.1021/acsenergylett.6c00594
ACS Energy Lett. 2026, 11, 4457−4464

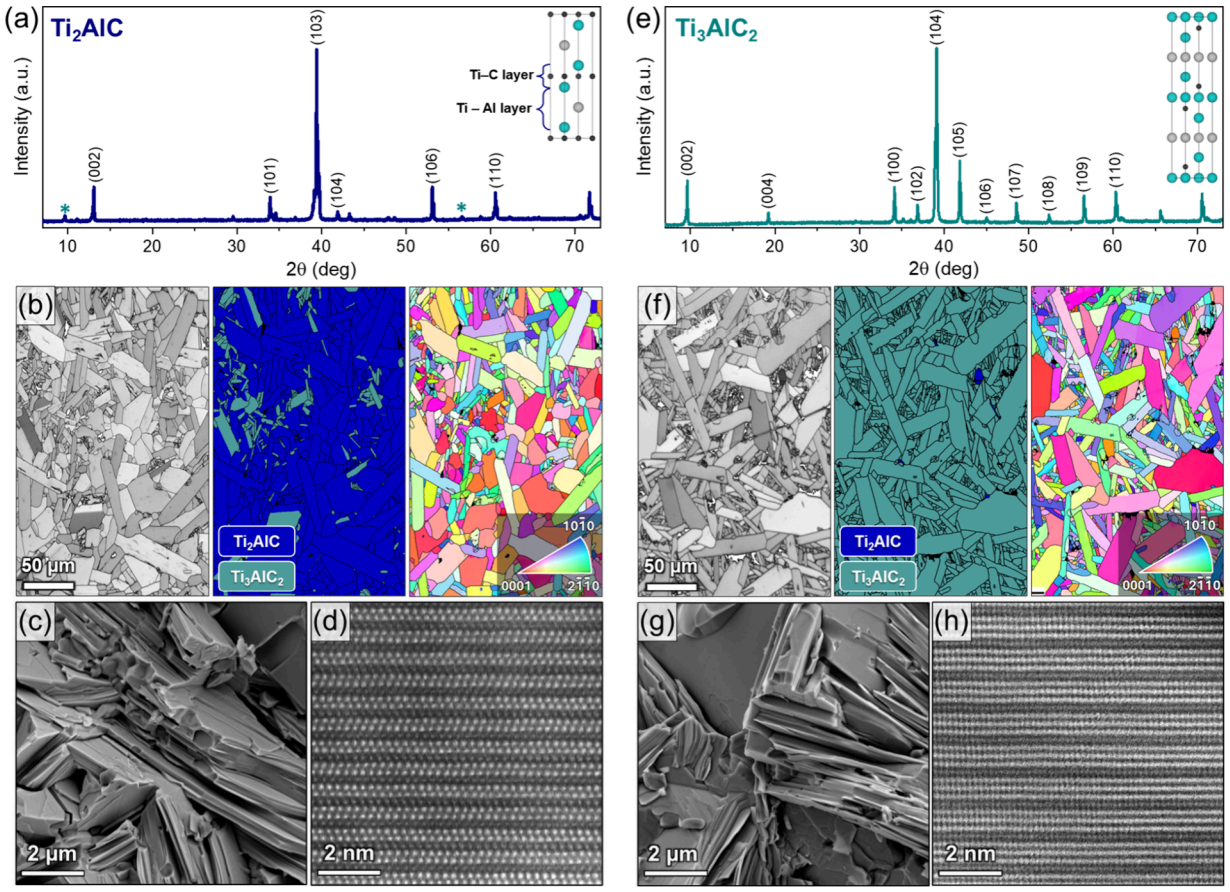


Figure 1. Characterization of Ti_2AlC (left) and Ti_3AlC_2 (right) MAX phases: (a and e) XRD patterns with a schematic of the lattice structure inset (Ti, teal; Al, gray; and C, black). The asterisk marks the (002) reflection of Ti_3AlC_2 found in Ti_2AlC. (b and f) EBSD analysis, including confidence index, phase, and IPF maps. (c and g) SEM image of the fractured surface. (d and h) atomically resolved HAADF−STEM images with bright intensity for the corresponding double and triple Ti layers between Al layers. The light C atomic columns are not revealed in the *Z*-contrast images recorded in $[2\bar{1}\bar{1}0]$ and $[01\bar{1}0]$ zone axes for Ti_2AlC and Ti_3AlC_2, respectively.

computational insights elucidate the atomic-scale mechanisms of hydrogen storage in MAX phases, experimental validation remains limited and restricted to gas-phase hydrogenation.[31−34]

Electrochemical hydrogen charging presents an attractive approach, enabling solid-state storage at ambient conditions[35−37] while also offering a more realistic experimental representation of application-relevant environments, such as coatings,[38−40] nuclear fuel cladding concepts,[41−43] and interconnects operating in hot corrosive[44,45] or fuel-cell electrolytes.[46,47] Despite the theory-backed potential of hydrogen storage in MAX phases, the fundamental trapping behavior by electrochemical hydrogen charging remains unexplored.

Herein, we present the first investigation into electrochemical hydrogen charging of MAX phases, comparing the two most common types, with similar chemistry but different ratios of metal/carbide interfaces: Ti_2AlC and Ti_3AlC_2. Hydrogen diffusion was assessed via Kelvin probe measurements, and the desorption mechanisms were studied using both thermal desorption spectroscopy (TDS) and electrochemical methods. These experiments, together with density functional theory (DFT) calculations, enabled us to identify the behavior of the different trapping sites and reveal their relation to the proportion of metal and carbide layers.

Ti_2AlC and Ti_3AlC_2 ceramics were produced by spark plasma sintering (SPS) as described in the Experimental Section. X-ray diffraction (XRD) patterns show successful synthesis of both phases (Figure 1a and e), although a small amount of Ti_3AlC_2 (∼10 vol %) is present in the Ti_2AlC samples (which is common for Ti_2AlC synthesized by SPS[48,49]). The microstructures analyzed via scanning electron microscopy (SEM) are comparable, comprising of similar average grain sizes (∼20 μm) with elongated morphologies and minimal (<1%) residual porosity (Figure 1b and f). The different phases are revealed by electron backscatter diffraction (EBSD) phase maps, while inverse pole figure (IPF) maps showcase heterogeneous orientation distributions with no strong texture (Figure 1b and f). Fractured surface SEM examination (Figure 1c and g) showcases the typical MAX phase plate-like lamellar structure. The corresponding atomic layer stacking of Ti and Al can be clearly identified by atomically resolved high-angle annular dark-field (HAADF) scanning transmission electron microscopy (STEM) imaging (Figure 1d and h), where the different ratios of the metal/carbide interface can be seen for each phase: two layers of carbide per metal layer and three layers of carbide per metal layer in Ti_2AlC and Ti_3AlC_2, respectively.

Electrochemical hydrogen charging was evaluated using a three-electrode cell configuration (Figure 2a) under acidic conditions (1 M H_2SO_4), with a reversible hydrogen electrode

https://doi.org/10.1021/acsenergylett.6c00594
ACS Energy Lett. 2026, 11, 4457−4464

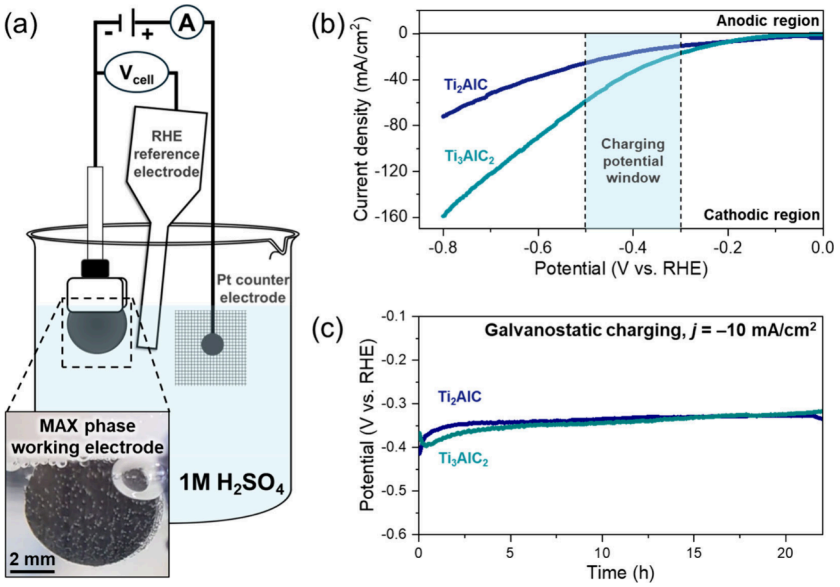


Figure 2. (a) Schematic of the three-electrode cell setup comprising the MAX phase working electrode, RHE reference electrode, and Pt mesh counter electrode, in a 1 M H_2SO_4 electrolyte. A photograph of a MAX phase working electrode during hydrogen charging is shown. (b) LSV curves under HER conditions, comparing Ti_2AlC and Ti_3AlC_2. (c) Evolution of potential during galvanostatic hydrogen charging, showing minimal changes during the process.

(RHE), Pt mesh counter electrode, and MAX phase disc-shaped working electrode (6.5 mm in diameter and ∼1 mm thickness). Linear sweep voltammetry (LSV) shown in Figure 2b was used to determine the charging window. The cathodic charging current density was set to 10 mA/cm^2 to ensure sufficient charging rates while minimizing interference or damage stemming from bubble accumulation, impeding the electrode active surface, in addition to using a magnetic stirrer. The galvanostatic experiments were set for 24 h, during which potential profiles were measured (Figure 2c). The potential remains stable after an initial activation period and displays only a slight change over an extended charging duration, suggesting that both materials maintain steady hydrogen adsorption without significant surface passivation. Bubble formation is limited to small surface bubbles, as shown in Figure 2a, which indicates that the selected charging conditions allow hydrogen uptake while keeping the active area largely accessible.

Hydrogen desorption behavior was studied using TDS and cyclic voltammetry (CV). Ti_2AlC and Ti_3AlC_2 samples were charged for 24 h prior to desorption experiments under identical conditions. TDS was performed up to 600 °C at a heating rate of 4 °C min^{-1}, followed by a final isothermal hold at 600 °C to complete hydrogen desorption. The TDS spectra for both phases (Figure 3a and b) shows two well-defined desorption peaks at about 300 and 600 °C. The first peak is indicative of intermediate trapping sites, requiring less thermal energy for desorption. The desorption temperature of this peak correlates with previous studies on gas phase hydrogenated Mg/MAX-phase composites,[31,50] where the desorption was measured up to 350 °C. The second desorption peak appears at a relatively high temperature, indicating the existence of deep trapping sites in the materials. Note that these release temperatures exceed the desired range for mobile applications, but are comparable to strongly bound metal hydride systems,[10,11] remaining relevant for stationary storage or controlled released applications.

To electrochemically assess hydrogen release pathways, CV was recorded after the charging step, a well-tested approach to reveal Heyrovsky-like desorption,[51−53] and compared to a CV recorded prior to the charging. The scans were collected between 0 and 1 V vs RHE, a region free of significant faradaic contributions, as shown in the unbroken voltammograms in Figure 3c and d, so that any current response arises from hydrogen desorption alone. Voltammograms extending to cathodic potentials (Figure S1) confirm the absence of major faradaic processes within the selected operation window. The initial cycle prior to charging shows a minor feature at ∼0.3−0.4 V, attributed to surface redox processes.[54,55] After charging, two pronounced broad desorption peaks appear at approximately 0.3 and 0.7 V for both phases. These signals correspond to hydrogen release and closely mirror the behavior observed by TDS (Figure 3a−d). The agreement between the electrochemical and thermal signatures indicates that both phases store hydrogen in comparable states, with a distinct preferential site governing storage in each one of the phases. In Ti_2AlC, the intermediate traps dominate the desorption response, whereas in Ti_3AlC_2, the deep traps are more prominent (Figure 3a−d). Cycling experiments (Figure S2) show that the trapping sites remain stable during cycling and exhibit the same observed trend for each MAX phase. Negligible changes in the overall storage capacities are observed after three charging−electrochemical desorption cycles. Post-charging characterization by XPS indicates negligible changes to the MAX phase surfaces, with partial reduction of the few nanometer native oxide layer (Figure S3). Additionally, XRD on samples subjected to multiple charging/desorption cycles (both electrochemical and thermal desorption) shows that no detectable structural changes occur in the MAX phases (Figure S4).

Diffusion and trapping behavior were assessed by KP measurements (Figure 3e), further supporting the observed trends. The evolution of the surface potential reveals that hydrogen breakthrough occurs earlier in Ti_2AlC than in Ti_3AlC_2, corresponding to apparent hydrogen diffusion

https://doi.org/10.1021/acsenergylett.6c00594
ACS Energy Lett. 2026, 11, 4457−4464

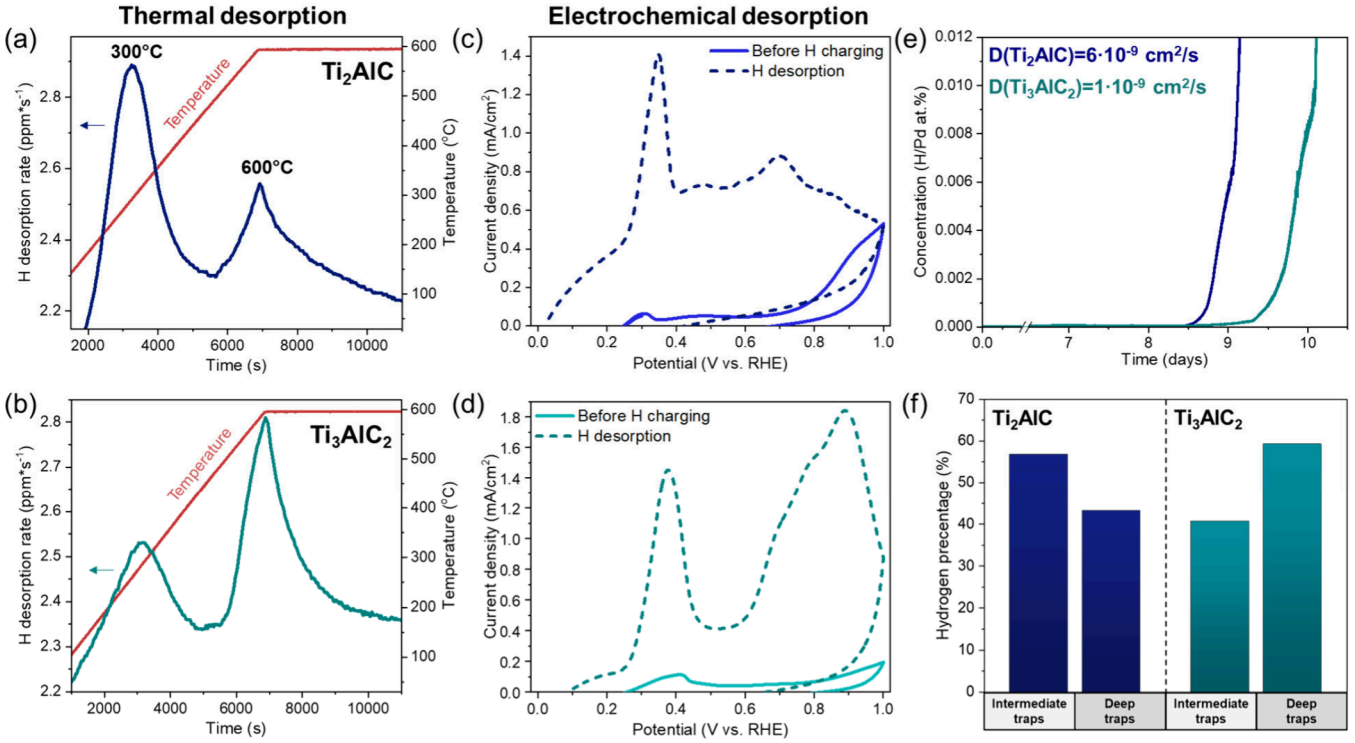


Figure 3. Hydrogen desorption analysis in Ti_2AlC (top) and Ti_3AlC_2 (bottom) MAX phases after 24 h of hydrogen charging. (a and b) Thermal desorption spectroscopy, showcasing two distinct peaks at approximately 300 and 600 °C. (c and d) Cyclic voltammograms of the hydrogen desorption region, presenting the same trend seen by TDS; two distinct peaks at 0.3 and 0.7 V vs RHE. (e) Permeation curves obtained by the Kelvin probe for Ti_2AlC and Ti_3AlC_2. Diffusion coefficients were calculated according to the breakthrough time presented in the plot. (f) Percentage of hydrogen in intermediate and deep traps for each phase, showcasing an opposite trend.

coefficients of 6×10^{-9} and 1×10^{-9} cm^2 s^{-1}, respectively. Compared to reported hydrogen diffusivities for electrochemically charged metal hydrides[56−58] and TiC_x[52,59,60] systems, the values determined here indicate kinetically accessible hydrogen transport for both phases; however, direct comparison remains limited by scarce data in the literature and differing experimental conditions. The slower diffusion in Ti_3AlC_2 is consistent with the higher fraction of deep traps seen in the desorption experiments, supporting that hydrogen is more strongly trapped in Ti_3AlC_2, whereas Ti_2AlC facilitates faster transport through a higher proportion of shallower trapping sites. It is worth noting that, according to the KP measurements, 24 h of charging is not enough to reach hydrogen saturation.

Desorption data was analyzed to calculate the amount of trapped hydrogen and quantitively compare the hydrogen percentage in the different kinds of trapping sites in both MAX phases. After 24 h of charging, Ti_2AlC and Ti_3AlC_2 stored approximately 0.15 and 0.18 wt %, respectively. These fractions are of the same order of magnitude as previously reported for Ti_2AlC under gas hydrogenation.[61] In Ti_2AlC, roughly 60% and 40% of hydrogen desorbed from intermediate and deep traps, respectively, whereas the inverse trend of 40% and 60% is observed for Ti_3AlC_2 (Figure 3f). These opposite proportions can be attributed to the difference in the Ti−C (carbide) to Ti−Al (metal) layer ratio (i.e., higher n value in $Ti_{n+1}AlC_n$) and their characteristic trapping sites, elucidating which traps are more prevalent in either phase. Thus, it is hypothesized that intermediate traps are associated with interstitial sites in the M−A (Ti−Al) layers, while deep traps are related to carbon vacancies within the M−X (Ti−C) layers. These types of trapping sites have been previously proposed in theoretical studies on hydrogen in MAX phases.[29,30,62] Furthermore, MAX phases with higher n values reportedly exhibit an increased tendency for X vacancy formation,[63−69] which promotes deep hydrogen trapping.[62,70] As a result, Ti_3AlC_2 shows a higher fraction of deeply trapped hydrogen, whereas Ti_2AlC, with a higher density of Ti−Al interfaces, favors shallow trapping. These observations strongly suggest that hydrogen trapping in MAX phases is governed by interstitial sites within the Ti−A layer and hydrogen occupation of carbon vacancy sites within the carbide layers.

Building on these experimental results, DFT calculations were performed for Ti_2AlC and Ti_3AlC_2, to quantify hydrogen trapping energies and identify preferred interstitial sites. Using $2 \times 2 \times 1$ supercells, four possible different interstitial hydrogen (H) occupation sites were studied (Figure 4a and b): a tetrahedral site consisting of 3 Ti atoms and 1 Al atom (position 1), a tetrahedral site consisting of 3 Al atoms and 1 Ti atom (position 2), an octahedral site consisting of 3 Ti and 3 Al atoms (position 3), and a tetrahedral site consisting of 4 Ti atoms, where H lies in a C layer (position 4). Corresponding ground state (0 K) formation energies are shown in Table 1. The interstitial sites in the Ti−Al interlayer are energetically preferred for both phases, with position 1 being the most favorable. In the case of the H atom located in the Ti−C layer (position 4), it relaxes to the Ti−Al interlayer interstitial positions, which indicates that Ti−C interlayer interstitial positions are generally unstable and tend to remain unoccupied. In all cases, the insertion of a single hydrogen atom into the interstitial sites causes only negligible changes in the lattice parameters (Table S1).

https://doi.org/10.1021/acsenergylett.6c00594
ACS Energy Lett. 2026, 11, 4457−4464

The behavior of H atoms in the presence of vacancies was examined in the framework of the dilute limit using 4 × 4 × 1 supercells. Vacancy formation energies for both phases are summarized in Table S2, with Ti_3AlC_2 (2.63 eV) exhibiting lower values than Ti_2AlC (3.15 eV) for C vacancies, consistent with previous studies.[29,30] Upon the introduction of a H atom to the direct vicinity of a preformed C vacancy, the H atom relaxes into the vacancy site, occupying the empty position in the C sublattice. A comparison of these binding energies to those of the interstitial sites in the Ti−Al interlayers (Table 1) shows that H within the C vacancies is bound more strongly than in the interstitial sites.

DFT results indicate that Ti_2AlC predominantly accommodates hydrogen in weakly bound interstitial sites within the Ti−Al interlayers, facilitating easier release. In Ti_3AlC_2, Ti−Al interlayer interstitials are similarly favored; however, the higher availability of C vacancies alongside the lower formation energy increases the possibility of their existence within the framework, prompting hydrogen to occupy the empty sites within the Ti−C layers. Hydrogen atoms bound at these C-vacancy sites exhibit substantially higher binding energies, requiring greater energy for their desorption, consistent with the experimental observations from TDS and CV.

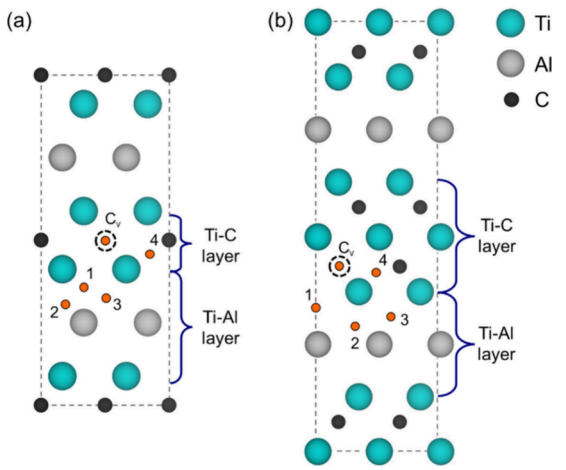


Figure 4. Schematic representation of investigated interstitial positions and C vacancies (C_v) for H incorporation in (a) Ti_2AlC and (b) Ti_3AlC_2.

Table 1. Ground State Formation Energies (E_f) of H Incorporation at Different Interstitial Sites and a Single-Point Defect (C Vacancy) in Ti_2AlC and Ti_3AlC_2, According to DFT Calculations[a]

	E_f (eV)	
H position	Ti_2AlC	Ti_3AlC_2
1	−0.36	−0.31
2	−0.27	−0.20
3	−0.27	−0.20
4	−0.36	−0.31
C vacancy	−0.83	−0.98

[a]Note that all sites adsorb hydrogen exothermically.

Our findings confirm that hydrogen storage in MAX phases occurs through trapping sites intrinsic to their atomically layered structure, which remain stable over repeated charging cycles. These trapping sites are determined by the MAX phase structure and chemistry, which differ from classic defect-based trapping sites observed in metals (e.g., grain boundaries and dislocations) or microstructure-dependent hydride formation. This structural origin of trapping offers routes to enhance hydrogen uptake via stable and microstructure-independent trapping site engineering enabled by the high tunability of MAX phases:[26,71,72] M-, A-, and X-site disordered solid solutions,[73,74] ordered solid solutions (i.e., o-max and i-max),[75−78] high entropy,[79−81] and ordered vacancies,[82] to name but a few several possibilities. For example, studies have shown that alloying MAX phases can markedly enhance the hydrogen storage capacity in M-site[61] and A-site[30] solid solutions. Although the gravimetric capacity and kinetics of traditional $Ti_{n+1}AlC_n$ MAX phases remain insufficient for practical hydrogen storage applications, they provide a well-defined model system for experimentally distinguishing trapping mechanisms associated with M−A and M−X layers. Ultimately, tailoring MAX phases through their structure, chemistry, and defects could potentially enable higher capacity, improved kinetics, and effective hydrogen release at lower temperatures.

In summary, we demonstrate electrochemical hydrogen charging of Ti_2AlC and Ti_3AlC_2 MAX phases, studying the difference in hydrogen behavior between these materials. Hydrogen diffusion in the MAX phases under electrochemical charging conditions (measured by KP) exhibited apparent diffusion rates on the order of 10^{-9} cm^2 s^{-1}. These moderately slow rates coupled with the trapping sites observed by TDS are indicative of a trapping-limited diffusion behavior. Thermal and electrochemical desorption analysis (by TDS and CV) revealed two distinct trap types in both MAX phases, an intermediate trap desorbing at ∼300 °C and a deep trap above 600 °C. Although the trapping sites are seemingly identical, their relative contribution presented a noticeably different trend for each phase, ∼60% intermediate traps and ∼40% deep traps for Ti_2AlC and vice versa in Ti_3AlC_2. The presence of multiple trapping sites, each with their distinct desorption temperatures, reflects inherent characteristic traps, which, on the one hand, impede rapid hydrogen release but, on the other hand, suggest potential tunability through MAX phase engineering. The observed traps can be attributed to interstitial sites in the Ti−Al layers (intermediate traps) and carbon vacancies within the Ti−C carbide layer (deep traps), consistent with the different metal/carbide layer ratios in each phase. DFT calculations show that the interstitial sites have a lower binding energy (−0.20 to −0.36 eV) than C vacancies (−0.83 to −0.98 eV), while C vacancy formation is more favorable in Ti_3AlC_2 than Ti_2AlC (2.63 and 3.15 eV, respectively). This is in full agreement with the observations made by desorption experiments, further supporting the existence of two different trapping sites. More broadly, the combined experimental observations and DFT calculations demonstrate that hydrogen storage and release in MAX phases are inherently trapping dominated, offering a foundation for engineering trap-controlled hydrogen storage in atomically layered materials.

■ ASSOCIATED CONTENT

Supporting Information

The Supporting Information is available free of charge at https://pubs.acs.org/doi/10.1021/acsenergylett.6c00594.

https://doi.org/10.1021/acsenergylett.6c00594
ACS Energy Lett. 2026, 11, 4457−4464

Experimental section, computational details, additional supporting experimental data of Ti_2AlC and Ti_3AlC_2, including CVs, XRD, and XPS spectra (Figures S1−S4), and additional computational data (Tables S1 and S2) (PDF)

AUTHOR INFORMATION

Corresponding Authors

Rebeca Miyar − *Max Planck Institute for Sustainable Materials, 40237 Düsseldorf, Germany*; orcid.org/0009-0002-2792-9680; Email: r.miyar@mpi-susmat.de

Maria Jazmin Duarte − *Max Planck Institute for Sustainable Materials, 40237 Düsseldorf, Germany*; Email: j.duarte@mpi-susmat.de

Authors

Adam C. Miles − *Max Planck Institute for Sustainable Materials, 40237 Düsseldorf, Germany*

Michal Fečík − *Materials Chemistry, RWTH Aachen University, 52074 Aachen, Germany*; orcid.org/0000-0001-9342-3923

Manoj Prabhakar − *Max Planck Institute for Sustainable Materials, 40237 Düsseldorf, Germany*

Guillaume Hachet − *Max Planck Institute for Sustainable Materials, 40237 Düsseldorf, Germany; Université de Rouen Normandie, CNRS, INSA Rouen Normandie, Groupe de Physique des Matériaux UMR 6634, F-76000 Rouen, France*

Lilian Vogl − *Max Planck Institute for Sustainable Materials, 40237 Düsseldorf, Germany*

Dierk Raabe − *Max Planck Institute for Sustainable Materials, 40237 Düsseldorf, Germany*

Gerhard Dehm − *Max Planck Institute for Sustainable Materials, 40237 Düsseldorf, Germany*

Yug Joshi − *Max Planck Institute for Sustainable Materials, 40237 Düsseldorf, Germany*

Maxim Sokol − *Department of Materials Science and Engineering, Tel Aviv University, Ramat Aviv 6997801, Israel*; orcid.org/0000-0001-8588-0585

Jochen M. Schneider − *Materials Chemistry, RWTH Aachen University, 52074 Aachen, Germany*; orcid.org/0000-0003-1239-1961

Barak Ratzker − *Max Planck Institute for Sustainable Materials, 40237 Düsseldorf, Germany*; orcid.org/0000-0003-0242-1282

Complete contact information is available at: https://pubs.acs.org/10.1021/acsenergylett.6c00594

Funding

Open access funded by Max Planck Society.

Notes

The authors declare no competing financial interest.

ACKNOWLEDGMENTS

This work has been performed in the framework of the International Max Planck Research School for Sustainable Metallurgy (IMPRS SusMet). M.F. and J.M.S. gratefully acknowledge the computing time provided to them at the NHR Center NHR4CES at RWTH Aachen University (Project p0020883). This is funded by the Federal Ministry of Research, Technology and Space and the State Governments Participating on the Basis of the Resolutions of the GWK for National High-Performance Computing at Universities (www.nhr-verein.de/unsere-partner). B.R. acknowledges the support of an Alexander von Humboldt fellowship. The authors thank Zakarya Meshou for overall laboratory support and Benjamin Breitbach for support with XRD measurements.

REFERENCES

(1) Fang, W.; Ding, C.; Chen, L.; Zhou, W.; Wang, J.; Huang, K.; Zhu, R.; Wu, J.; Liu, B.; Fang, Q.; Wang, X.; Wang, J. Review of Hydrogen Storage Technologies and the Crucial Role of Environmentally Friendly Carriers. *Energy Fuels* **2024**, *38* (15), 13539−13564.

(2) Sattar, M. A.; Rasul, M. G.; Jahirul, M. I.; Hasan, M. M. An Up-to-Date Review on the Progress and Challenges of Hydrogen Storage, and Its Safety and Economic Analysis. *Sustain. Energy Fuels* **2024**, *8* (16), 3545−3573.

(3) Sun, H.; Wang, Z.; Meng, Q.; White, S. Advancements in Hydrogen Storage Technologies: Enhancing Efficiency, Safety, and Economic Viability for Sustainable Energy Transition. *Int. J. Hydrogen Energy* **2025**, *105*, 10−22.

(4) Miskan, S. N.; Abdulkadir, B. A.; Setiabudi, H. D. Materials on the Frontier: A Review on Groundbreaking Solutions for Hydrogen Storage Applications. *Chemical Physics Impact* **2025**, *10*, 100862.

(5) Reilly, J. J.; Sandrock, G. D. Hydrogen Storage in Metal Hydrides. *Sci. Am.* **1980**, *242* (2), 118.

(6) Sakintuna, B.; Lamari-Darkrim, F.; Hirscher, M. Metal Hydride Materials for Solid Hydrogen Storage: A Review. *Int. J. Hydrogen Energy* **2007**, *32* (9), 1121−1140.

(7) Qureshi, F.; Yusuf, M.; Ahmed, S.; Haq, M.; Alraih, A. M.; Hidouri, T.; Kamyab, H.; Vo, D. V. N.; Ibrahim, H. Advancements in Sorption-Based Materials for Hydrogen Storage and Utilization: A Comprehensive Review. *Energy* **2024**, *309*, No. 132855.

(8) Lang, C.; Jia, Y.; Yan, X.; Ouyang, L.; Zhu, M.; Yao, X. Molecular Chemisorption: A New Conceptual Paradigm for Hydrogen Storage. *Chem. Synth.* **2022**, *2*, 1.

(9) Dornheim, M.: Tailoring Reaction Enthalpies of Hydrides. In *Handbook of Hydrogen Storage: New Materials for Future Energy Storage*; Hirscher, M., Ed.; Wiley: Hoboken, NJ, 2010; Chapter 7, pp 187−214, DOI: 10.1002/9783527629800.ch7.

(10) Ward, P. A.; Corgnale, C.; Teprovich, J. A.; Motyka, T.; Hardy, B.; Sheppard, D.; Buckley, C.; Zidan, R. Technical Challenges and Future Direction for High-Efficiency Metal Hydride Thermal Energy Storage Systems. *Appl. Phys. A: Mater. Sci. Process.* **2016**, *122* (4), 462.

(11) Dubey, S. K.; Ravi Kumar, K.; Tiwari, V.; Srivastva, U. Impacts, Barriers, and Future Prospective of Metal Hydride-Based Thermochemical Energy Storage System for High-Temperature Applications: A Comprehensive Review. *Energy Technology* **2024**, *12* (4), No. 2300768.

(12) Allendorf, M. D.; Stavila, V.; Snider, J. L.; Witman, M.; Bowden, M. E.; Brooks, K.; Tran, B. L.; Autrey, T. Challenges to Developing Materials for the Transport and Storage of Hydrogen. *Nature Chemistry* **2022**, *14* (11), 1214−1223.

(13) Lim, K. L.; Kazemian, H.; Yaakob, Z.; Daud, W. R. W. Solid-State Materials and Methods for Hydrogen Storage: A Critical Review. *Chem. Eng. Technol.* **2010**, *33* (2), 213−226.

(14) Drawer, C.; Lange, J.; Kaltschmitt, M. Metal Hydrides for Hydrogen Storage − Identification and Evaluation of Stationary and Transportation Applications. *J. Energy Storage* **2024**, *77*, No. 109988.

(15) Alobaid, A.; Kamil, M.; Abdelrazek Khalil, K. Metal Hydrides for Solid Hydrogen Storage: Experimental Insights, Suitability Evaluation, and Innovative Technical Considerations for Stationary and Mobile Applications. *Int. J. Hydrogen Energy* **2025**, *128*, 432−456.

(16) Wei, F. G.; Tsuzaki, K. Quantitative Analysis on Hydrogen Trapping of TiC Particles in Steel. *Metallurgical and Materials Transactions A* **2006**, *37* (2), 331−353.

(17) Takahashi, J.; Kawakami, K.; Kobayashi, Y. Origin of Hydrogen Trapping Site in Vanadium Carbide Precipitation Strengthening Steel. *Acta Mater.* **2018**, *153*, 193−204.

(18) Shi, R.; Ma, Y.; Wang, Z.; Gao, L.; Yang, X. S.; Qiao, L.; Pang, X. Atomic-Scale Investigation of Deep Hydrogen Trapping in NbC/α-Fe Semi-Coherent Interfaces. *Acta Mater.* **2020**, *200*, 686−698.
(19) Chen, Y. S.; Lu, H.; Liang, J.; Rosenthal, A.; Liu, H.; Sneddon, G.; McCarroll, I.; Zhao, Z.; Li, W.; Guo, A.; Cairney, J. M. Observation of Hydrogen Trapping at Dislocations, Grain Boundaries, and Precipitates. *Science* **2020**, *367* (6474), 171−175.
(20) Zhang, B.; Zhu, Q.; Xu, C.; Li, C.; Ma, Y.; Ma, Z.; Liu, S.; Shao, R.; Xu, Y.; Jiang, B.; Gao, L.; Pang, X.; He, Y.; Chen, G.; Qiao, L. Atomic-Scale Insights on Hydrogen Trapping and Exclusion at Incoherent Interfaces of Nanoprecipitates in Martensitic Steels. *Nat. Commun.* **2022**, *13* (1), 3858.
(21) Deegan, M. M.; Lorzing, G. R.; Korman, K. J.; Rowland, C. A.; Dworzak, M. R.; Antonio, A. M.; Bloch, E. D. Hydrogen Storage in Porous Cages. *ACS Materials Au* **2023**, *3* (1), 66−74.
(22) Barsoum, M. W. The $M_{N+1}AX_N$ Phases: A New Class of Solids: Thermodynamically Stable Nanolaminates. *Prog. Solid State Chem.* **2000**, *28* (1−4), 201−281.
(23) Gonzalez-Julian, J. Processing of MAX Phases: From Synthesis to Applications. *J. Am. Ceram. Soc.* **2021**, *104* (2), 659−690.
(24) Sokol, M.; Natu, V.; Kota, S.; Barsoum, M. W. On the Chemical Diversity of the MAX Phases. *Trends Chem.* **2019**, *1* (2), 210−223.
(25) Barsoum, M. W.; El-Raghy, T. The MAX Phases: Unique New Carbide and Nitride Materials: Ternary ceramics turn out to be surprisingly soft and machinable, yet also heat-tolerant, strong and lightweight. *Am. Sci.* **2001**, *89* (4), 334−343.
(26) Dahlqvist, M.; Barsoum, M. W.; Rosen, J. MAX Phases − Past, Present, and Future. *Mater. Today* **2024**, *72*, 1−24.
(27) Wang, X. H.; Zhou, Y. C. Layered Machinable and Electrically Conductive Ti_2AlC and Ti_3AlC_2 Ceramics: A Review. *J. Mater. Sci. Technol.* **2010**, *26* (5), 385−416.
(28) Gonzalez-Julian, J. Processing of MAX Phases: From Synthesis to Applications. *J. Am. Ceram. Soc.* **2021**, *104* (2), 659−690.
(29) Ding, H.; Glandut, N.; Fan, X.; Liu, Q.; Shi, Y.; Jie, J. First-Principles Study of Hydrogen Incorporation into the MAX Phase Ti_3AlC_2. *Int. J. Hydrogen Energy* **2016**, *41* (15), 6387−6393.
(30) Das, P.; Thekkepat, K.; Lee, Y. S.; Lee, S. C.; Bhattacharjee, S. Computational Design of Novel MAX Phase Alloys as Potential Hydrogen Storage Media Combining First Principles and Cluster Expansion Methods. *Phys. Chem. Chem. Phys.* **2023**, *25* (6), 5203−5210.
(31) Wang, K.; Du, H.; Wang, Z.; Gao, M.; Pan, H.; Liu, Y. Novel MAX-Phase Ti_3AlC_2 Catalyst for Improving the Reversible Hydrogen Storage Properties of MgH_2. *Int. J. Hydrogen Energy* **2017**, *42* (7), 4244−4251.
(32) Tang, C.; Grosse, M.; Trtik, P.; Steinbrueck, M.; Stueber, M.; Seifert, H. J. H Permeation Behavior of Cr_2AlC and Ti_2AlC Max Phase Coated Zircaloy-4 by Neutron Radiography. *Acta polytechnica* **2018**, *58* (1), 69.
(33) Lakhnik, A. M.; Kirian, I. M.; Rud, A. D. The Mg/MAX-Phase Composite for Hydrogen Storage. *Int. J. Hydrogen Energy* **2022**, *47* (11), 7274−7280.
(34) Duan, X.-Q.; Li, G.-X.; Zhang, W.-H.; Luo, H.; Tang, H.-M.; Xu, L.; Sheng, P.; Wang, X.-H.; Huang, X.-T.; Huang, C.-K.; Lan, Z.-Q.; Zhou, W.-Z.; Guo, J.; Ismail, M. B.; Liu, H.-Z. Ti_3AlCN MAX for Tailoring MgH_2 Hydrogen Storage Material: From Performance to Mechanism. *Rare Metals* **2023**, *42* (6), 1923−1934.
(35) Gholami, T.; Pirsaheb, M. Review on Effective Parameters in Electrochemical Hydrogen Storage. *Int. J. Hydrogen Energy* **2021**, *46* (1), 783−795.
(36) Xu, X.; Dong, Y.; Hu, Q.; Si, N.; Zhang, C. Electrochemical Hydrogen Storage Materials: State-of-the-Art and Future Perspectives. *Energy Fuels* **2024**, *38* (9), 7579−7613.
(37) Lahrar, E. H.; El Harrak, A.; Faik, A. Electrochemical Hydrogen Storage: Critical Parameters and Performance Drivers. *J. Power Sources* **2025**, *658*, No. 238481.
(38) Ma, G.; Zhang, A.; Wang, Z.; Wang, K.; Zhang, J.; Xu, K.; Xu, Y.; Zhou, S.; Wang, A. MAX Phase Coatings: Synthesis, Protective Performance, and Functional Characteristics. *Mater. Horiz.* **2025**, *12* (6), 1689−1710.
(39) Wang, Z.; Ma, G.; Li, Z.; Ruan, H.; Yuan, J.; Wang, L.; Ke, P.; Wang, A. Corrosion Mechanism of Ti_2AlC MAX Phase Coatings under the Synergistic Effects of Water Vapor and Solid NaCl at 600 °C. *Corros. Sci.* **2021**, *192*, No. 109788.
(40) Wang, Q. M.; Flores Renteria, A.; Schroeter, O.; Mykhaylonka, R.; Leyens, C.; Garkas, W.; to Baben, M. Fabrication and Oxidation Behavior of Cr_2AlC Coating on Ti6242 Alloy. *Surf. Coat. Technol.* **2010**, *204* (15), 2343−2352.
(41) Gigax, J. G.; Kennas, M.; Kim, H.; Wang, T.; Maier, B. R.; Yeom, H.; Johnson, G. O.; Sridharan, K.; Shao, L. Radiation Response of Ti_2AlC MAX Phase Coated Zircaloy-4 for Accident Tolerant Fuel Cladding. *J. Nucl. Mater.* **2019**, *523* (1), 26−32.
(42) Xiao, Y.; Xiao, H.; Mo, T.; Ren, L.; Tian, Y.; Zhu, L. High-Temperature and Interfacial Oxidation of MAX Phase-Reinforced Composite Coatings Deposited by Laser Cladding on Zr Alloy Substrates. *Ceram. Int.* **2023**, *49* (23), 38672−38682.
(43) Yunus, M.; Maji, B. C. Synthesis and Thermal Stability of High-Purity Cr_2AlC MAX-Phase for Accident Tolerant Fuel Cladding Application. *Ceram. Int.* **2025**, *51* (29), 60767−60778.
(44) Prikhna, T. A.; Ostash, O. P.; Kuprin, A. S.; Podhurska, V. Y.; Serbenyuk, T. B.; Gevorkyan, E. S.; Rucki, M.; Zurowski, W.; Kucharczyk, W.; Sverdun, V. B.; Karpets, M. V.; Ponomaryov, S. S.; Vasyliv, B. D.; Moshchil, V. E.; Bortnitskaya, M. A. A New MAX Phases-Based Electroconductive Coating for High-Temperature Oxidizing Environment. *Compos. Struct.* **2021**, *277*, No. 114649.
(45) Li, J. J.; Li, M. S.; Xiang, H. M.; Lu, X. P.; Zhou, Y. C. Short-Term Oxidation Resistance and Degradation of Cr_2AlC Coating on M38G Superalloy at 900−1100 °C. *Corros. Sci.* **2011**, *53* (11), 3813−3820.
(46) Lu, J. L.; Abbas, N.; Tang, J. N.; Tang, J.; Zhu, G. M. Synthesis and Characterization of Conductive Ceramic MAX-Phase Coatings for Metal Bipolar Plates in Simulated PEMFC Environments. *Corros. Sci.* **2019**, *158* (1), No. 108106.
(47) Madhavan, P. V.; Zeng, X.; Shahgaldi, S.; Li, X. Investigation of Cr_2SiC Ceramic MAX Phase Coated Metallic Bipolar Plates in Ex-Situ Conditions for Proton Exchange Membrane Fuel Cells. *Int. J. Hydrogen Energy* **2024**, *96*, 1232−1242.
(48) Zhou, W. B.; Mei, B. C.; Zhu, J. Q.; Hong, X. L. Rapid Synthesis of Ti_2AlC by Spark Plasma Sintering Technique. *Mater. Lett.* **2005**, *59* (1), 131−134.
(49) Wang, X. H.; Zhou, Y. C. Layered Machinable and Electrically Conductive Ti_2AlC and Ti_3AlC_2 Ceramics: A Review. *J. Mater. Sci. Technol.* **2010**, *26* (5), 385−416.
(50) Lakhnik, A. M.; Kirian, I. M.; Rud, A. D. The Mg/MAX-Phase Composite for Hydrogen Storage. *Int. J. Hydrogen Energy* **2022**, *47* (11), 7274−7280.
(51) Lebègue, E. Allen J. Bard, Larry. R. Faulkner, Henry S. White: Electrochemical Methods: Fundamentals and Applications, 3rd edition, Wiley. *Transit. Met. Chem.* **2023**, *48*, 433−436.
(52) Gringoz, A.; Glandut, N.; Valette, S. Electrochemical Hydrogen Storage in $TiC_{0.6}$, Not in $TiC_{0.9}$. *Electrochem. commun.* **2009**, *11* (10), 2044−2047.
(53) Uluc, A. V.; Mol, J. M. C.; Terryn, H.; Böttger, A. J. Hydrogen Sorption and Desorption Related Properties of Pd-Alloys Determined by Cyclic Voltammetry. *J. Electroanal. Chem.* **2014**, *734*, 53−60.
(54) Tian, L.; Li, Y.; Ju, P.; Fu, C.; Wang, E.; Zhao, G. Enhanced Strength and Corrosion Resistance of Macro-Porous Ti_3AlC_2 with High Porosity by Introducing Glassy Carbon. *Ceram. Int.* **2022**, *48* (7), 9890−9896.
(55) Gandara, M.; Mladenović, D.; Oliveira Martins, M. J.; Rakocevic, L.; Kruszynski de Assis, J. M.; Šljukić, B.; Sarmento Gonçalves, E. MAX Phase (Nb_4AlC_3) For Electrocatalysis Applications. *Small* **2024**, *20* (29), No. 2310576.
(56) Cui, N.; Luo, J. L. Electrochemical Study of Hydrogen Diffusion Behavior in Mg_2Ni-TYPE Hydrogen Storage Alloy Electrodes. *Int. J. Hydrogen Energy* **1999**, *24* (1), 37−42.

https://doi.org/10.1021/acsenergylett.6c00594
ACS Energy Lett. 2026, 11, 4457−4464

(57) Feng, F.; Han, J.; Geng, M.; Northwood, D. O. Study of Hydrogen Transport in Metal Hydride Electrodes Using a Novel Electrochemical Method. *J. Electroanal. Chem.* **2000**, *487* (2), 111−119.
(58) Kazakov, A. N.; Blinov, D. V.; Bodikov, V. Y.; Mitrokhin, S. V.; Volodin, A. A. Hydrogen Storage and Electrochemical Properties of Annealed Low-Co AB5 Type Intermetallic Compounds. *Int. J. Hydrogen Energy* **2021**, *46* (25), 13622−13631.
(59) Nguyen, J.; Glandut, N.; Jaoul, C.; Lefort, P. Electrochemical Hydrogen Insertion in Substoichiometric Titanium Carbide $TiC_{0.6}$: Influence of Carbon Vacancy Ordering. *Langmuir* **2013**, *29* (38), 12036−12042.
(60) Nguyen, J.; Glandut, N.; Jaoul, C.; Lefort, P. Hydrogen Insertion in Substoichiometric Titanium Carbide. *Int. J. Hydrogen Energy* **2015**, *40* (27), 8562−8570.
(61) De, S. K.; Bhattacharyya, S. Hydrogen Adsorption by a Porous Bimetallic Solid Solution Carbide MAX Phases Synthesized in an Open Atmosphere. *J. Energy Storage* **2023**, *73*, No. 109009.
(62) Fu, Y.; Li, Z.; Gao, W.; Zhao, D.; Huang, Z.; Sun, B.; Yan, M.; Liu, G.; Liu, Z. Exploring Hydrogen Incorporation into the Nb_4AlC_3 MAX Phases: Ab Initio Calculations. *Materials* **2022**, *15* (21), 7576.
(63) Tzenov, N. V.; Barsoum, M. W. Synthesis and Characterization of Ti_3AlC_2. *J. Am. Ceram. Soc.* **2000**, *83* (4), 825−832.
(64) Music, D.; Ahuja, R.; Schneider, J. M. Theoretical Study of Nitrogen Vacancies in Ti_4AlN_3. *Appl. Phys. Lett.* **2005**, *86* (3), 031911.
(65) Du, Y. L.; Sun, Z. M.; Hashimoto, H.; Tian, W. B. First-Principles Study of Carbon Vacancy in Ta_4AlC_3. *Mater. Trans.* **2008**, *49* (9), 1934−1936.
(66) Music, D.; Riley, D. P.; Schneider, J. M. Energetics of Point Defects in TiC. *J. Eur. Ceram. Soc.* **2009**, *29* (4), 773−777.
(67) Eklund, P.; Beckers, M.; Jansson, U.; Högberg, H.; Hultman, L. The $M_{n+1}AX_n$ Phases: Materials Science and Thin-Film Processing. *Thin Solid Films* **2010**, *518* (8), 1851−1878.
(68) Barsoum, M. W: *MAX Phases: Properties of Machinable Ternary Carbides and Nitrides*; Wiley-VCH Verlag GmbH & Co. KGaA: Weinheim, Germany, 2013; DOI: 10.1002/9783527654581.
(69) Zhang, H.; Hu, T.; Wang, X.; Zhou, Y. Structural Defects in MAX Phases and Their Derivative MXenes: A Look Forward. *J. Mater. Sci. Technol.* **2020**, *38*, 205−220.
(70) Ling, W.; Lai, K.; Chen, J.; Guo, F.; Kang, D.; Zhao, Z.; Dai, J. Point Defects and Hydrogen-Permeation Behavior of MAX Phase Cr_2AlC Coating by First-Principles Studies. *Nuclear Materials and Energy* **2023**, *36*, No. 101486.
(71) Sokol, M.; Natu, V.; Kota, S.; Barsoum, M. W. On the Chemical Diversity of the MAX Phases. *Trends Chem.* **2019**, *1* (2), 210−223.
(72) Serafin, J.; Dziejarski, B.; Oindo Achieng, G.; Vendrell, X.; Chaitoglou, S.; Amade-Rovira, R. Comprehensive Analysis of MAX Phase and MXene Materials for Advanced Photocatalysis, Electrocatalysis and Adsorption in Hydrogen Evolution and Storage. *Journal of Industrial and Engineering Chemistry* **2025**, *142* (2), 18−33.
(73) Kubitza, N.; Büchner, C.; Sinclair, J.; Snyder, R. M.; Birkel, C. S. Extending the Chemistry of Layered Solids and Nanosheets: Chemistry and Structure of MAX Phases, MAB Phases and MXenes. *ChemPlusChem* **2023**, *88* (8), e202300214.
(74) Dahlqvist, M.; Rosen, J. Combined In- and out-of-Plane Chemical Ordering in Super-Ordered MAX Phases (s-MAX). *Nanoscale* **2025**, *17* (22), 13787−13796.
(75) Dahlqvist, M.; Petruhins, A.; Lu, J.; Hultman, L.; Rosen, J. Origin of Chemically Ordered Atomic Laminates (i-MAX): Expanding the Elemental Space by a Theoretical/Experimental Approach. *ACS Nano* **2018**, *12* (8), 7761−7770.
(76) Xiao, P.; Jin, N.; Lin, Z. Double Transition Metal-Containing M_2TiAlC_2 o-MAX Phases as Li-Ion Batteries Anodes: A Theoretical Screening. *Mater. Res. Lett.* **2021**, *9* (12), 516−522.
(77) Feng, X.; Li, N.; Chen, B.; Zeng, C.; Bai, T.; Wu, K.; Cheng, Y.; Xiao, B. Thermodynamics for the Non-Conventional Synthesizing of out-of-Plane Ordered Double-Transition Metal "312" and "413" MAX Phases (o-MAX): A High Throughput Linear Programing First-Principles Calculation. *J. Mater. Sci. Technol.* **2023**, *134*, 81−88.
(78) Makani, N. H.; Rai, B. K.; Bastakoti, B. P.; Bretana, A.; Gautam, B. Current Advances in I-MAX Phases and Their Two Dimensional Derivative i-MXenes: Challenges and Opportunities. *Adv. Electron. Mater.* **2025**, *11* (21), No. e00478.
(79) Du, Z.; Wu, C.; Chen, Y.; Zhu, Q.; Cui, Y.; Wang, H.; Zhang, Y.; Chen, X.; Shang, J.; Li, B.; Chen, W.; Liu, C.; Yang, S. High-Entropy Carbonitride MAX Phases and Their Derivative MXenes. *Adv. Energy Mater.* **2022**, *12* (6), No. 2103228.
(80) Xiao, H.; Zhao, S.; Liu, Q.; Li, Y.; Zhao, S.; Luo, F.; Wang, Y.; Huang, Q.; Wang, C. Point Defect Properties in High Entropy MAX Phases from First-Principles Calculations. *Acta Mater.* **2023**, *248*, No. 118783.
(81) Tian, Z.; Hu, F.; Zhang, P.; Fan, Y.; Shamshirgar, A. S.; Wu, S.; Cai, L.; Bai, Y.; Wu, X.; Rosen, J.; Sun, Z. M. High-Entropy Engineering of A-Site in MAX Phases toward Superior Microwave Absorption Properties. *Matter* **2025**, *8* (12), 102367.
(82) Oliveira, F. M.; Amousa, N.; Subramani, A.; Luxa, J.; Senthil, C.; Sofer, Z.; Gonzalez-Julian, J. Maximizing Potential Applications of MAX Phases: Sustainable Synthesis of Multielement Ti_3AlC_2. *Inorg. Chem.* **2024**, *63* (32), 14851.

https://doi.org/10.1021/acsenergylett.6c00594
ACS Energy Lett. 2026, 11, 4457−4464